Variations in Cathodoluminescent Intensity of Spacecraft Materials Exposed to Energetic Electron Bombardment

Justin Dekany, Justin Christensen, JR Dennison,
Amberly Evans Jensen, Gregory Wilson, Todd Schneider, Charles W. Bowers and Robert Meloy

***Abstract*—Many contemporary spacecraft materials exhibit cathodoluminescence when exposed to electron flux from the space plasma environment. A quantitative, physics-based model has been developed to predict the intensity of the glow as a function of incident electron current density and energy, temperature, and intrinsic material properties. We present a comparative study of the absolute spectral radiance for several types of dielectric and composite materials based on this model which spans three orders of magnitude. Variations in intensity are contrasted for different electron environments, different sizes of samples and sample sets, different testing and analysis methods, and data acquired at different test facilities. Together, these results allow us to estimate the accuracy and precision to which laboratory studies may be able to determine the response of spacecraft materials in the actual space environment. It also provides guidance as to the distribution of emissions that may be expected for sets of similar flight hardware under similar environmental conditions.**

***Index Terms*—cathodoluminescence, light emission, materials testing, electron flux, space environment effects**

I. INTRODUCTION

Many highly disordered insulating materials used in spacecraft construction can exhibit electron-induced glow or cathodoluminescence when exposed to the space plasma environment [1]. Determinations of the absolute and relative cathodoluminescent intensity of spacecraft materials per incident electron flux are essential to predict and mitigate consequences for optical detection [2] and for stray light contamination in space-based observatories [1,3]. They also provide important information about the defect structure and electron transport properties of these materials [4-8].

Previous studies have focused on how the relative spectral radiance of cathodoluminescent materials varies with changes in environmental conditions, including electron energy, current density, absorbed power density, and temperature. This has led to the development of a quantitative, physics-based model to predict the intensity of glow as a function of incident electron current density and energy, temperature, and intrinsic material properties [1,3,7,9]. However, from a practical point of view, it is also important to develop an understanding of the variations of the cathodoluminescent intensity of diverse spacecraft materials exposed to energetic electron bombardment in both the space environment and space simulation studies. This is the focus of this paper.

We present results of ground-based measurements simulating space-induced cathodoluminescence from a wide variety of thin film dielectric and nanodielectric composite samples. Comparisons of the absolute spectral intensities per incident electron flux for these materials show three orders of magnitude variation. Variations in intensity are contrasted for different incident electron current densities and energies, different sample sizes and thicknesses, different testing and analysis methods, and data acquired at different test facilities. We also report on the variability of cathodoluminescence for a large set of similar epoxy samples exposed simultaneously to similar space-like monoenergetic electron flux conditions. The observed statistical fluctuations provide assessment of the instrumentation precision, the variation between samples, and the stochastic variations inherent to the material. The combined results of studies of numerous similar samples led to higher precision results that allow for quantification of additional materials properties.

II. MODEL OF CATHODLUMINESCENT INTENSITY

The model developed for the observed electron-induced luminescence phenomenon is based on band theory of highly disordered insulating materials [3,7,10]. The observed luminescence occurs when an incident high energy, charged particle undergoes a series of inelastic collisions exciting valence band electrons into the conduction band. The excited electrons rapidly decay to localized (shallow trapped) states, with a mean binding energy ε_{ST} below the mobility edge. A final electron transition, from the short-lived shallow trap states to longer-lived deep trap states is the origin of the emitted photon. The model predicts that the overall luminescencent intensity I_γ scales with incident current density

Research was conducted in the Environment Effects Laboratory at NASA Marshall Space Flight Center and in the Space Environment Effects Materials (SEEM) test facility at Utah State University. The studies were supported by funding from the NASA Goddard Space Flight Center. Additional support was provided by the Air Force Research Laboratory through a National Research Council Senior Research Fellowship for Dennison and a NASA Space Technology Research Fellowship for Jensen.

Justin Dekany (e-mail: JDekany.phyx@gmail.com), Justin Christensen (e-mail: J.Christensen@aggiemail.usu.edu), Amberly Evans Jensen (e-mail: Amb.Eva@aggiemail.usu.edu), Greg Wilson (e-mail: GregDWilson@gmail.com) and JR Dennison (e-mail: JR.Dennison@usu.edu) are with the Materials Physics Group in the Physics Department at Utah State University in Logan, UT 84322 USA.

Todd Schneider is with the Environment Effects Branch at NASA Marshall Space Flight Center in Huntsville, AL (e-mail: Todd.Schneider@nasa.gov)

Charles W. Bowers is with NASA Goddard Space Flight Center in Greenbelt, MD. (e-mail: Charles.W.Bowers@nasa.gov)

Robert Meloy is with ASRC Federal Space and Defense, Inc in Greenbelt, MD. (e-mail: Robert.M.Meloy@nasa.gov)

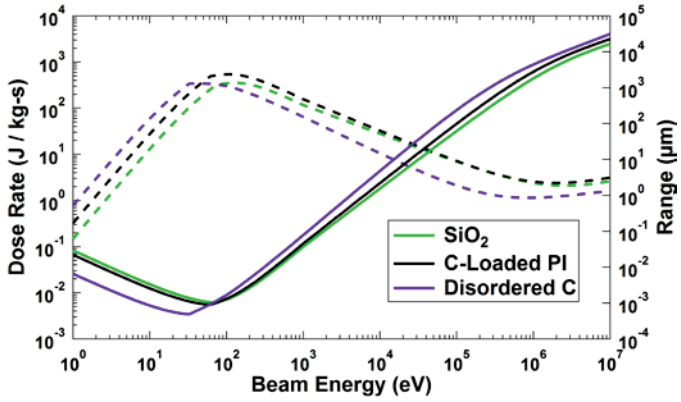

Fig. 1. Range (solid curves) and dose rate (dashed curves) of three disordered materials (SiO_2, carbon-loaded polyimide, and graphitic amorphous carbon) as a function of incident electron energy using calculation methods and the continuous slow-down approximation described in Wilson *et al*. [14].

J_{inc}, incident beam energy E_{inc}, temperature T, and photon wavelength λ as

$$I_\gamma(J_{inc}, E_{inc}, T, \lambda) \propto \frac{\dot{D}(J_{inc}, E_{inc})}{\dot{D} + \dot{D}_{sat}} \left\{\left[e^{-(\varepsilon_{ST}/k_B T)}\right]\left[1 - e^{-(\varepsilon_{ST}/k_B T)}\right]\right\} \times \left\{\left[1 - \mathbb{A}_f(\lambda)\right]\left[1 + \mathbb{R}_m(\lambda)\right]\right\} . \quad (1)$$

The dose rate $\dot{D}$ (absorbed power per unit mass) is given by

$$\dot{D}(J_{inc}, E_{inc}) = \frac{J_{inc} E_{inc}[1-\eta(E_{inc})]}{q_e \rho_m} \times \begin{cases} [1/L] & ; R(E_{inc}) < L \\ [1/R(E_{inc})] & ; R(E_{inc}) > L \end{cases} . \quad (2)$$

q_e is the electron charge, ρ_m is the mass density of the material, $\eta(E_b)$ is the contribution of backscattered yield, and L is the sample thickness. $\dot{D}_{sat}$ is the material-dependent saturation dose rate. The exponential terms in Eq. (1) account for temperature dependence [3]. The last two λ-dependant terms correct for photon absorption within the luminescent material and reflection from any underlying coating [11]. A more detailed discussion of the model is given in [1]. This work focuses on the dependence of spectral radiance on J_{inc}, E_{inc}, and the range of the deposited electrons, $R(E_{inc})$.

The dependence of the spectral radiance on incident current density, J_{inc}, in Eq.(1) is through the dependence on dose rate; $I_\gamma(J_{inc}) \propto \dot{D}(J_{inc})/[D(\dot{J}_{inc}) + \dot{D}_{sat}] \propto J_{inc}/[J_{inc} + J_{sat}]$. At low dose rates ($\dot{D} \ll \dot{D}_{sat}$), I_γ is linearly proportional to J_{inc}. At higher current densities ($\dot{D} \gg \dot{D}_{sat}$), saturation occurs when trap states fill, limiting the number of states electrons can decay into; I_γ approaches a constant material-specific saturation intensity. Such saturation effects, at increasing current densities and fixed incident energies, have been reported for disordered SiO_2 [3], nanodielectric carbon-loaded polyimide [9], cynate ester/graphite fiber composites [12], and bisphenol/amine epoxy [1,13].

The energy dependence of the spectral radiance is more complicated, due to the energy-dependent penetration depth or range, $R(E_{inc})$, in Eq. (2). For nonpenetrating radiation—where the energy-dependent penetration depth or range, $R(E_{inc})$, is less than the film thickness L—all incident power is absorbed in the material. At low incident power, both $\dot{D}$ and I_γ are linearly proportional to the incident energy and power density, $(J_{inc}E_{inc}/q_e)$. At higher incident power, both $\dot{D}$ and I_γ exhibit saturation effects for increasing energy and fixed current density. For penetrating radiation—where $R(E_{inc}) > L$—the *absorbed* power is reduced by a factor of $[L/R(E_{inc})]$ [14] leading to a similar dependence for I_γ. Fig. 1 shows the range and dose for select disordered materials as functions of incident energy.

An energy-dependent correction to the incident flux, $J_{inc}[1-\eta(E_{inc})]$, is also included in Eq. (2) to account for quasi-elastic backscattered electrons that do not deposit substantial energy; $\eta(E_{inc})$ is the backscattered electron yield [11]. For the most part, this correction is small and weakly dependant on energy. For biased samples, or when excess charge is stored in the trap states, a surface voltage V_s results and E_{inc} is replaced everywhere in Eqs. (1) and (2) by the landing energy, $(E_{inc} - q_e V_s)$.

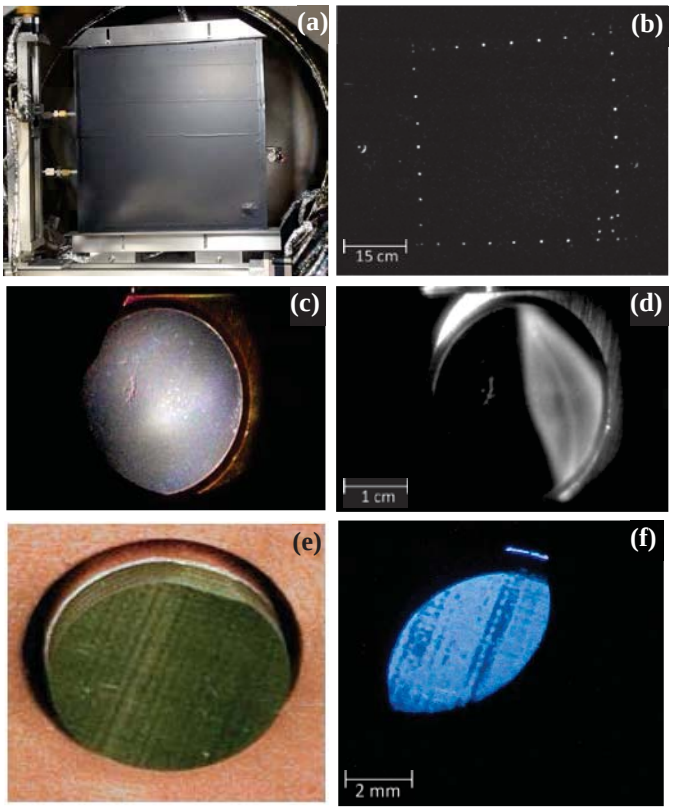

Fig. 2. Sample images in ambient light (left) and under electron bombardment (right) showing variations in sample composition, size and facility. **(a-b)** 41x41 cm sample of carbon-loaded polyimide mounted in the MSFC test chamber, with 36 epoxy glue dots luminescing under electron flux. **(c-d)** 2.5 cm diameter sample of thin disordered SiO_2 coating on Au-coated mirror mounted in the USU SEEM test chamber. **(d)** Image with the beam focus adjusted so that electrons impinge and cathodoluminescence is evident only on the right side of the sample. **(e-f)** 1 cm diameter sample of cynate ester/graphite fiber composite at USU. Striations in the images result from the composite fiber structure of the material. **(f)** Image with the electron beam offset to the top left, limiting cathodoluminescence to this quadrant. **(b)** and **(d)** are CCD video frame images; all other images are SLR still color photographs.

III. Cathodoluminescent Variations

A. *Experimental Test Methods and Facilities*

Cathodoluminescence tests used well-characterized, uniform, large-area, approximately normal-incidence, monochromatic electron beams to irradiate tests samples. The

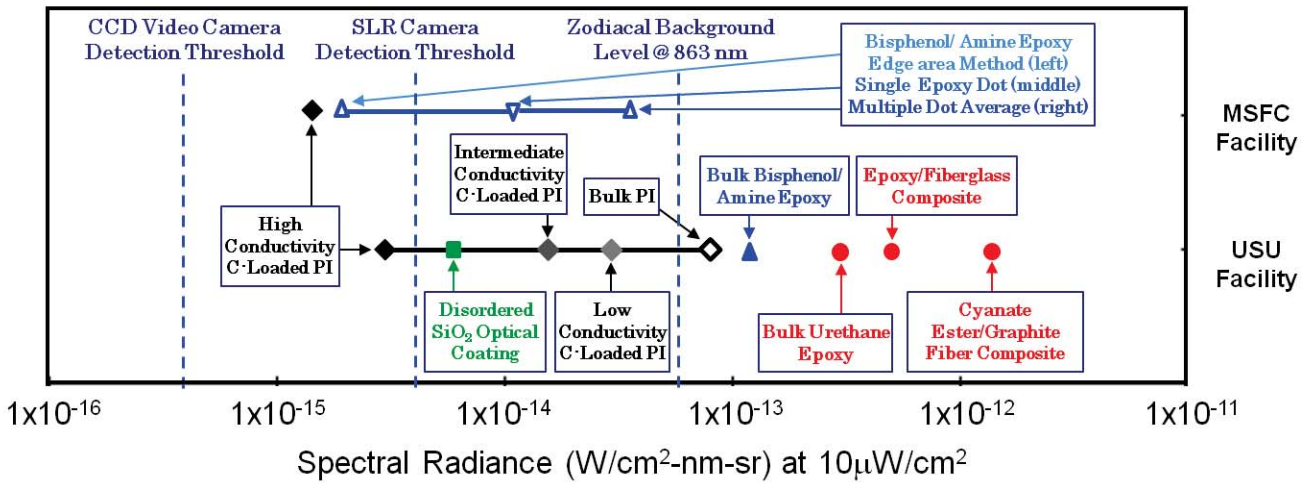

Fig. 3. Measured absolute cathodoluminescent intensities for ~10 keV electron bombardment scaled to 10 μW/cm^2, representative of severe space environments. Data acquired using the CCD video camera (863 nm weighted central wavelength and 500 nm bandwidth). The materials shown—in approximate order of increasing intensity—are: three levels of decreasing carbon loading of polyimide from high to low conductivity and bulk polyimide (black squares); disordered SiO_2 optical coatings (green); neat bisphenol/amine and urethane epoxies (blue); and composite resin fiber materials including cyanate ester/ graphite fiber, urethane epoxy/carbon fiber, and epoxy/fiberglass composites (red);. Measurements at the two test facilities are identified at right. Three data analysis methods are compared for bisphenol/amine samples; these range over more than two orders of magnitude, illustrating the need for well designed test methods. The spectral radiance for the zodiacal background stray light intensity at 863 nm is shown for comparison (dashed blue line) [17], as are the detection thresholds of the cameras at the MSFC facility [1].

samples were in high vacuum conditions, held at fixed temperatures that could be controlled to cryogenic levels. Results presented here used two optical detectors: (i) an image-intensified CCD video camera (Xybion, ISG-780-U-3; ~400-900 nm bandwidth and 830 nm peak wavelength), and (ii) a single lens reflex CCD still camera (Cannon, EOS Rebel XT DS126071; ~390-650 nm bandwidth and 553 nm peak wavelength) [1]. The cameras were calibrated on an absolute scale using NIST traceable sources; their detection threshold sensitivities are noted in Fig. 3. In addition to the optical detectors, picoammeters measured current through the sample, monitored the mounting stage current, and measured beam currents.

Figure 2 shows some examples of materials tested and CCD video camera and SLR still camera color images of the cathodoluminescence. In Fig. 2(d) cathodoluminescence is evident only on the right side of the SiO_2 sample, where the beam has been focused. Figure 2(f) of a cynate ester/graphite fiber composite sample shows a uniform circular electron beam offset to the top left, limiting cathodoluminescence to this quadrant.

Measurements were conducted at two independent facilities: the Environment Effects Laboratory at NASA Marshall Space Flight Center (MSFC) and the Space Environment Effects Materials (SEEM) test facility at Utah State University (USU).

USU testing uses a ~1 m^3 ultrahigh vacuum chamber (~10^{-6} Pa) equipped with a high energy electron gun with a focused beam (5-30 keV at 0.1-1000 nA/cm^2 flux) [15]. Temperatures from ~50 K to ~350 K were used for cathodoluminescence tests [16]. Samples from <1 cm to ~3 cm diameter were tested. Additional NIR-IR and mid-IR cameras and detectors, UV/Vis/NIR spectrometers, and electron emission measurement capabilities were used for some measurements [1].

MSFC testing used a larger ~2 m x 1 m diameter ultrahigh vacuum chamber (~10^{-6} Pa) able to accommodate large (up to 41x41 cm) flight samples. It is equipped with a high energy electron flood gun (1-100 keV at 1-100 nA/cm^2 flux) with *in situ* Faraday cups positioned on either side of the large sample to monitor the incident beam current (see Fig. 2(a)). Temperatures down to ~120 K were attained by mounting samples on an electrically-isolated liquid nitrogen reservoir.

Measurements at the two test facilities are identified separately in Fig. 3. Measurements for similar materials (bisphenol/amine and intermediate conductivity carbon-loaded polyimide samples) show agreement to within a factor of ~2-3. This is reasonable agreement given the differences in sample materials, temperatures, test methods, instrumentation, and electron bombardment conditions for the different tests. However, it also serves as an indication of the uncertainties associated with ground-based testing.

B. Variations with Material

Figure 3 show a comparison of measured absolute cathodoluminescent spectral radiances for different spacecraft materials, which spans approximately three orders of magnitude. These different results for varied current, keV electron bombardment have been linearly scaled to 10 μW/cm^2 incident electron power densities, which is representative of severe space environments. The materials tested include: polyimide films, neat urethane and bisphenol/amine epoxy films; bulk and thin optical coatings of disordered SiO_2; several grades of commercially available high-conductivity carbon-loaded polyimide nanodielectric composites; cyanate ester and urethane epoxy resins in graphite fiber and fiberglass composites; and multilayer dielectric/conductor composites.

In general terms, we found that the relative cathodoluminescence for a given electron flux ranks from lowest to highest intensity for polyimide nanodielectric composites, disordered SiO_2, bulk polyimide, bulk epoxy materials, and epoxy resin composites. Polyimide and carbon-loaded polyimide exhibit relatively weak cathodoluminescent intensities, with the intensity decreasing with carbon content. As a point of comparison, note that these absolute spectral

intensities for isolated samples exposed to electron fluxes comparable to solar wind intensities span the intensity of the zodiacal background in the visible and near infrared wavelength range (vertical dashed line of Fig. 3) [17]; this relative comparison of intensities to the zodiacal background is most important for space-based observatories, where the zodiacal background can be a significant source of external light contamination [1]. Also note that these measured intensities are greater than the scaled CCD video camera detection threshold.

Figure 4 shows three cathodoluminescence spectra typical of spacecraft materials which are all similar in the visible region, and exhibit multiple peaks indicative of multiple types of defects. The cynate ester [12] and SiO_2 [3] spectra were acquired at USU; the epoxy spectra is from a different facility [6].

C. Variation with Energy and Penetration Depth

The energy dependence of cathodoluminescence scales as a saturation function of the dose rate (see Eq. (1)) For nonpenetrating radiation, the dose rate (see Eq. (2)) scales linearly with energy with a small—usually negligible—correction term for the energy dependence of the electron backscatter yield. Figure 5 shows spectral radiance versus incident energy curves for two bulk materials—cynate ester/graphite fiber composite (red circle) [12], and bisphenol/amine epoxy (blue triangles) [13]—where the sample is thick enough that all the incident electrons are deposited. These increase linearly with energy at low incident power density, but reach saturation limits at higher power densities (~10^3 μW/cm^2 for the cynate ester and ~230 μW/cm^2 (±70%) for bisphenol materials). The bisphenol data fit by the linear curve in Fig. 5 (blue triangles) does not show appreciable saturation, while other data (blue inverted triangles) shows significant saturation effects. Saturation of bisphenol/amine epoxy is also evident in Fig. 6 at lower power densities. The saturated spectral radiance curve (blue curve, with a saturation power density of 360 μW/cm^2 (±30%)) taken after the electron beam is turned on and after the sample has reached equilibrium deviates noticeably above ~50 μW/cm^2 from the linear spectral radiance curve (green curve) taken immediately after the electron beam is turned on and before saturation is reached.

For thin films, such as the ~60 nm SiO_2 optical coating in Fig. 5 (green curve), incident electrons above a threshold energy (~1.2 keV; see Fig.1)) are able to penetrate all the way through the material. For energies above this penetrating dose rate power deposition decreases with increasing energy, so the spectral radiance also decreases. Radiance from thicker SiO_2 layers is found to increase linearly to higher energies and at higher dose rates exhibit saturation effects [4].

With composite materials, such as the carbon-loaded polyimide, the relationship between energy and cathodoluminescent intensity is more complicated. The black

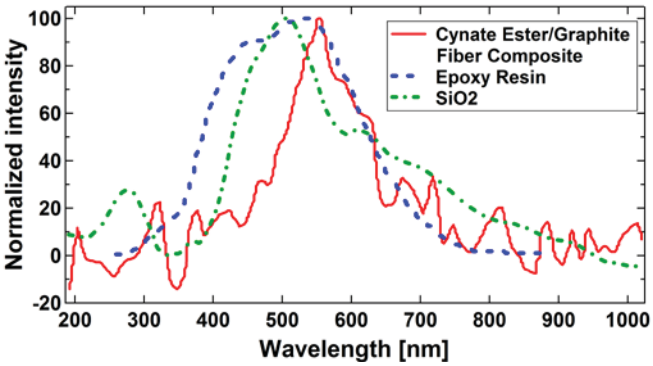

Fig. 4. Cathodoluminescent spectra of three highly disordered insulating materials. Materials shown are: cynate ester/graphite fiber composite (red solid curve) at ~100 K [12], epoxy resin at ~295 K (blue dashed curve) [6], and SiO_2-coated mirror at ~269 K (green dash-dotted curve) [3]. The spectra are normalized at maximum intensities and are not corrected for the wavelength-dependant relative detector sensitivity.

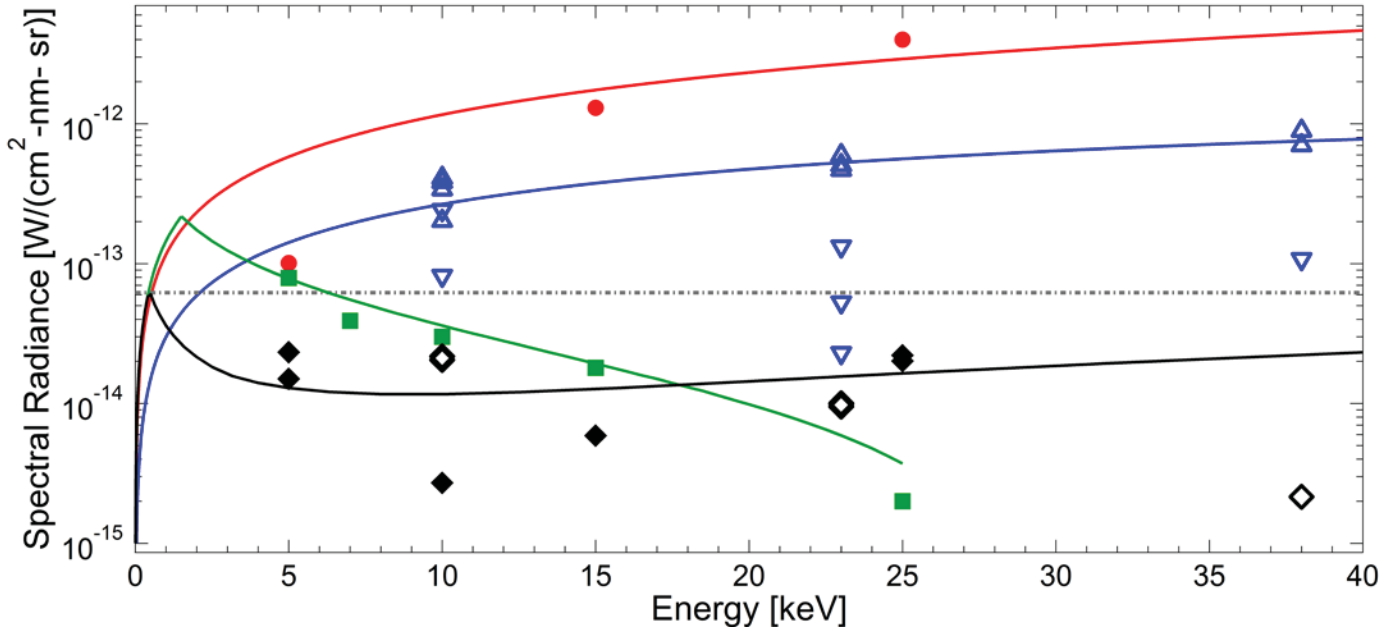

Fig. 5 Absolute cathodoluminescent spectral radiance versus incident electron energy of four materials, scaled to 10 nA/cm^2 electron current density. The plot shows data for SiO_2-coated mirror (green square) [3,4], carbon-loaded polyimide (black diamonds) [1,9], cynate ester/graphite fiber composite (red circle) [12], and bisphenol/amine epoxy (blue triangles) [1,13]. Data were taken with the CCD video camera at USU (solid symbols) and MSFC (open symbols). Fits are based on Eqs. (1) and (2). The approximate level of the zodiacal background stray light intensity at 863 nm is shown for comparison (dashed grey line) [17].

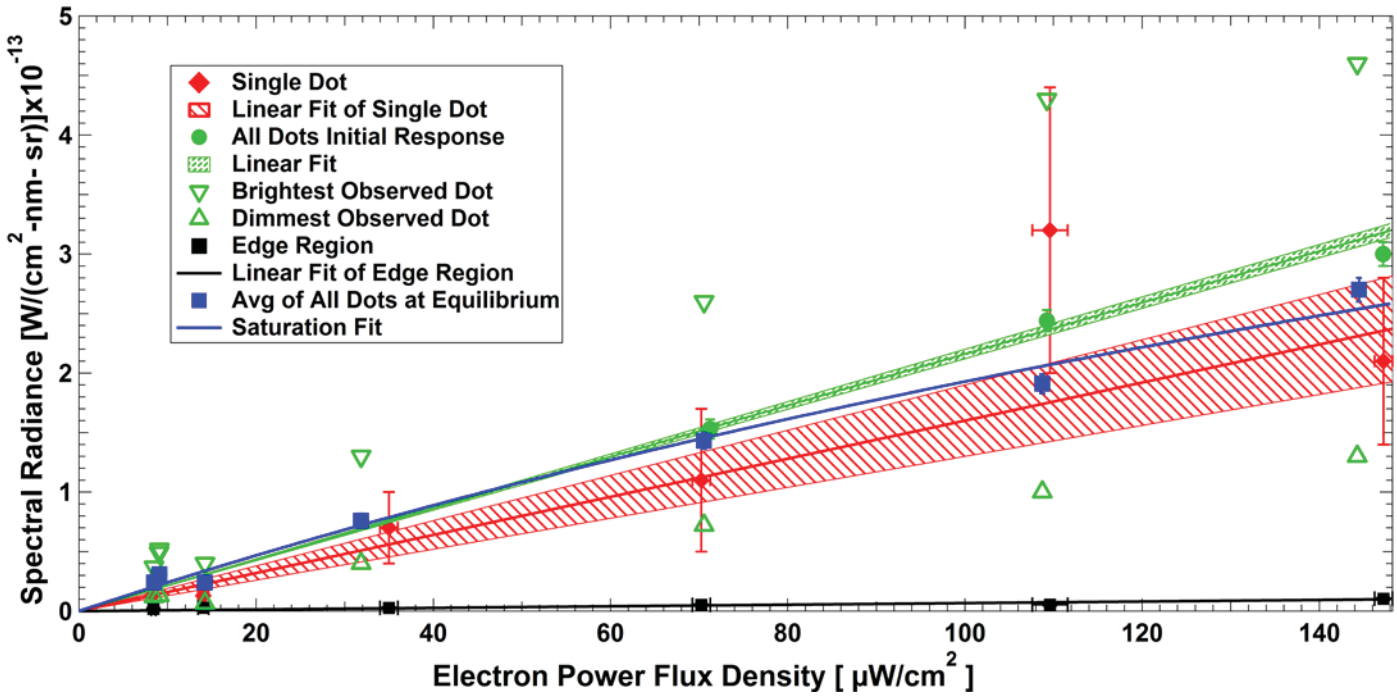

Fig. 6. Comparison of different methods to determine the absolute spectral radiance per incident electron power density as a function of incident electron energy for bulk bisphenol/amine epoxy samples. The slope of the linear fit, or conversion efficiency of high energy electron power to luminescent photon power, of 2.16 x 10^{-9} [W/(W-nm-sr)] (±2%) determined from the statistical analysis of 36 "glue dot" (green) is ~35% larger than from analysis of a single "glue dot" (red) and ~32X larger than from using edge region analysis (black). The range of variations of the 36 sample data set is indicated by the ~±5% standard deviation (error bars) and ~±60% minimum to maximum range (green triangles). Errors for the spectral radiance and slope values for the linear fit of the single "glue dot" are ~5X large than for the analysis of all dots. Comparison for the multiple sample data set of green initial (unsaturated) and blue equilibrium (saturated) curves show saturation effect at higher dose rates. The fit for the saturated (blue) curve from Eq. (1) is of the form $I_\gamma \propto \dot{D}/(\dot{D} + \dot{D}_{sat})$, with a proportionality constant of 9·10^{-13}[W/(cm^{2}nm·sr)] (±20%) and D_{sat}=1.5 kGy/s (±30%) or P_{sat}=360 μW/cm^2.

curve in Fig. 5. is a linear superposition with ~88% of a penetrating curve (10 nm thickness, with ~350 eV penetration energy) that models thin polyimide layers above carbon particles and ~12% of a nonpenetrating curve (2 μm thickness, with a penetration energy equal to the incident energy of ~10 keV) that models thick polyimide regions between the carbon particles. The relative surface areas of thin (~19%) and (~81%) thick polyimide regions determined with scanning electron microscopy are consistent with these estimates [18]. Even such a simple bimodal distribution of polyimide thicknesses predicts the relatively flat energy dependence of the spectral radiance curve observed at higher energies. A similar effect is seen qualitatively in Fig. 2(f) of the cynate ester/graphite fiber composite sample. Thicker regions of epoxy are lighter, while the thinner epoxy layers over graphite fibers are more intense and brighter blue in color.

D. Variations with Analysis Methods

Analysis of bisphenol/amine epoxy data taken at MSFC emphasizes the variation in results using three different analysis procedures [13]. Use of these different procedures to determine the absolute spectral radiance per incident electron power density as a function of incident electron energy, as shown in Fig. 6, produced results that differed by more than an order of magnitude.

The "edge region analysis" procedure defined a large square annular region that enclosed all 36 ~1 mm diameter "glue dot" regions of bulk epoxy as well as an ~220X larger area of surrounding carbon-loaded polyimide (see Fig. 2(b)). As expected and seen in Fig. 3, the estimated spectral radiance was much closer to that of carbon-loaded polyimide than bulk bisphenol/amine epoxy.

The "single dot analysis" procedure eliminated most of the contribution from carbon-loaded polyimide contamination by analyzing only a small region around a single epoxy dot. This procedure gives more accurate intensity results, but has a large statistical uncertainty since only ~15 pixels per frame comprising the single dot could be analyzed.

The most accurate results are obtained using the "multiple dot average" procedure. Data for all 36 epoxy dots individually are analyzed simultaneously using the single dot analysis; the statistical uncertainty is reduced by using the average value and associated standard deviation. As is readily apparent from Fig. 6, the multiple dot analysis results in much greater accuracy. Slopes of the linear fits in Fig. 6, or the spectral radiance per incident electron power density in [W/cm^2-nm-sr] per [μW/cm^2], measure the conversion efficiency of high energy electron power to luminescent photon power. The slope of 2.16 x 10^{-9} [W/(W-nm-sr)] (±2%) from the statistical analysis procedure (green) is ~35% larger than from the single dot analysis (red) and ~32X larger than from using edge region analysis (black). The multiple dot analysis result is the closet to the results measured at USU for a larger bulk sample, as shown in Fig. 2.

E. Variation of Similar Samples

Analysis multiple dots characterizes the variation between samples. The range of variations of the 36 sample data set is indicated by the ~±5% standard deviation (error bars) and ~±60% minimum to maximum range (triangles) shown in Fig.

6. The multiple dot analysis also results in much greater precision. Errors for the spectral radiance and slope values for the linear fit of the single dot procedure are ~5X large than for the analysis with the multiple dot procedure.

When many samples are statistically analyzed, precise measurements can be made at low intensities and additional small effects can become apparent. It is evident from comparison of the curves and associated uncertainties in Fig. 6 that the saturation effects discussed in Sec. III.C at low dose rates would not be observable without the higher precision obtained with the multiple dot procedure. That is, the observed differences for the green unsaturated curve and blue saturated curve are greater than the uncertainties in the red single dot curve. The uncertainty in $\dot{D}_{sat}$ was also reduce by more than a factor of 2.

IV. Conclusion

Cathodoluminescence is an important space environment-induced phenomenon to understand, especially in applications where extremely sensitive space-based optical detection is necessary. Measurements of the absolute spectral intensities per incident electron flux have been presented that confirm a quantitative, physics-based model to predict the intensity of the glow as a function of incident electron current density and energy, temperature, and sample thicknesses and composition. Comparisons for these materials show three orders of magnitude variation. For bulk nonpenetrating materials, spectral radiance increases with increasing incident electron power and flux. In thin films where electron penetration is possible, a linear relation is seen at low energies, but once penetration occurs intensity decreases with increasing energies. Composite materials, where both penetrating and nonpenetrating electrons effects were present, required a combination of these two effects in the model. Saturation effects at higher doses were observed and accurately modeled, for both penetrating and nonpenetrating electrons.

Statistical analysis of the observed statistical fluctuations of cathodoluminescence for a large set of similar epoxy samples exposed simultaneously to similar space-like monoenergetic electron flux conditions provided measures of both the instrumentation precision and the stochastic variations inherent to the material. The statistical analysis of the combined results of studies of numerous similar samples led to higher precision and accuracy results that allow for quantification of additional more subtle effects. Together, these results allow us to estimate the accuracy and precision to which laboratory studies may be able to determine the response of spacecraft materials in the actual space environment. It also provides guidance as to the distribution of emissions that may be expected for sets of similar flight hardware under similar environmental conditions.

Acknowledgement

Many members of the USU Materials Physics Group have contributed to the collective work which made this sumnative paper posibble. Discussions with the James Webb Space Telescope Spacecraft Charging Working Group have been most helpful in formulating the ideas presented here. We gratefully acknowledge Michael Taylor for the use of infrared and CCD video cameras.

References

[1] J.R. Dennison, A.E. Jensen, J. Dekany, G. Wilson, C.W. Bowers and R. Meloy, "Diverse Electron-induced Optical Emissions from Space Observatory Materials at Low Temperatures," *Proc. SPIE Cryogenic Optical Systems and Instr. Conf.*, Vol. 8863, 2013, pp. 88630B1-88630B15.

[2] D.C. Ferguson, J.-M. Krezan, D.A. Barton, J.R. Dennison, and S. Gregory, "On the Feasibility of Detecting Spacecraft Charging and Arcing by Remote Sensing," *J. Spacecraft and Rockets*, 2014, in press.

[3] A.E. Jensen, J.R. Dennison, G. Wilson, J. Dekany, C.W. Bowers, R. Meloy and J.B. Heaney, "Properties of Cathodoluminescence for Cryogenic Applications of SiO_2-based Space Observatory Optics and Coatings," *Proc. SPIE Cryogenic Optical Systems and Instr. Conf.*, Vol. 8863, 2013, pp. 88630A1-88630A10.

[4] A.E. Jensen and J.R. Dennison, "Defects Density of States Model of Cathodoluminescent Intensity and Spectra of Disordered SiO_2," *Proc. 13th Spacecraft Charging Techn. Conf.,* (Pasadena, CA, June, 2014).

[5] J.R. Dennison, J. Dekany, J.C. Gillespie, P. Lundgreen, A. Anderson, A.E. Jensen, G. Wilson, A.M. Sim, and R. Hoffmann, "Synergistic Models of Electron Emission and Transport Measurements of Disordered SiO_2," *Proc. 13th Spacecraft Charging Techn. Conf.,* (Pasadena, CA, June, 2014).

[6] G. Teyssedre, J. Franceschi, and C. Laurent, "Cathodo-and electro-luminescence spectra in insulating polymers: a parallel approach for inferring electrical ageing mechanisms." *Proc. IEEE-CEIDP*, pp. 824-827, 2007.

[7] G. Teyssedre, C. Laurent, G.C. Montanari, F. Palmieri, A. See, L.A. Dissado and J.C. Fothergill, "Charge distribution and electroluminescence in cross-linked polyethylene under dc field," J. Phys. D: Appl. Phys., **34,** 2830, 2001.

[8] H.-J. Fitting, T. Barfels, A. von Czarnowski, and A. N. Trukhin, "Electron Beam Induced Optical and Electronical Properties of SiO_2," Materials Science and Engineering, **B71**, 109-114 (2000).

[9] A.E. Jensen, J.R. Dennison, G. Wilson, and J. Dekany, "Nanodielectric Properties of High Conductivity Carbon-Loaded Polyimide Under Electron-Beam Irradiation," *Proc. 2013 IEEE Intern. Conf. on Solid Dielectrics (ICSD),* (Bologna, Italy, June, 2013), pp.730-735.

[10] A.M. Sim and J.R. Dennison, "Comprehensive Theoretical Framework for Modeling Diverse Electron Transport Experiments in Parallel Plate Geometries," Paper Number, AIAA-2013-2827, *5th AIAA Atmospheric and Space Environ. Conf.*, (San Diego, CA, June, 2013).

[11] J. R. Dennison, A. Evans, G. Wilson, J. Dekany, C. W. Bowers, and R. Meloy, "Electron Beam Induced Luminescence of SiO_2 Optical Coatings," Proc. IEEE-CEIDP (2012).

[12] J.A Roth, R. Hoffmann, and J.R. Dennison, "Effects of Radiation Induced Conductivity on Electrostatic Discharge in Insulating Materials," *Proc. 1st AIAA Atmospheric and Space Environments Conf.* (San Antonio, TX, 2009).

[13] J. Christensen, J. Dekany, and J.R. Dennison, "Stochastic Variations of Cathodoluminescent Intensity of Bisphenol/Amine Epoxy Exposed to Energetic Electron Bombardment," Utah State University Student Showcase, Logan, UT, April, 2014.

[14] G. Wilson and J.R. Dennison, "Approximation of Range in Materials as a Function of Incident Electron Energy," *IEEE Trans. on Plasma Sci.*, **40**(2), 305-310 (2012).

[15] W.Y. Chang, J.R. Dennison, N. Nickles and R.E. Davies, "Utah State University Ground-based Test Facility for Study of Electronic Properties of Spacecraft Materials," *Proc. 6th Spacecraft Charging Techn. Conf.*, (AFRL Sci. Center, Hanscom Air Force Base, MA, 2000).

[16] J. Dekany, R.H. Johnson, G. Wilson, A. Evans and J.R. Dennison, "Ultrahigh Vacuum Cryostat System for Extended Low Temperature Space Environment Testing," *Proc. 12th Spacecraft Charging Techn. Conf.,* (Kitakyushu, Japan, May, 2012).

[17] C. Leinert, *et al.*, "The 1997 Reference of Diffuse Night Sky Brightness," Astron. Astrophys. Suppl. Ser., **127**, 1, 1997.

[18] K. Peterson and J.R. Dennison, "Atomic Oxygen Modification of the Nanodielectric Surface Composition of Carbon-Loaded Polyimide Composites," Am. Phys. Soc. Four Corner Section Meeting, Denver, CO, October, 2013.

Justin Dekany is currently a graduate student at Utah State University in Logan, UT pursuing an MS in physics. He received a BS degree in physics from USU in 2010. He has worked with the Materials Physics Group for six years on electron transport measurements, electrostatic discharge tests, electron emission measurements, and luminescence studies related to spacecraft charging. He has been the Lab Manager for the Materials Physics Group for the last three years.

Justin Christensen is currently a senior, pursuing a BS in physics at Utah State University in Logan, UT. He has worked as an Undergraduate Research Assistant with the Materials Physics Group for a year. His work has focused on cathodoluminescent studies related to spacecraft charging.

Amberly Evans is currently a graduate student at Utah State University in Logan, UT pursing an MS in physics. She received BS degrees in physics and chemistry from USU in 2012. She has worked with the Materials Physics Group for seven years on electron emission, luminescence and resistivity studies and on MISSE retrieval and post-flight analysis of *SUSpECS*. Much of her work has focused on optical scattering and emission of spacecraft materials.

Greg Wilson is currently a graduate student at Montana State University in Bozeman, MT, pursuing a PhD in physics. He received BS degrees in physics and mathematics from Utah State University in Logan, UT in 2011 where he is completing his MS in physics. He has worked with the Materials Physics Group for three years on electron emission and luminescence studies related to spacecraft charging. He also developed a composite model for electron range over a wide range of incident energies applicable to diverse materials.

J. R. Dennison received the B.S. degree in physics from Appalachian State University, Boone, NC, in 1980, and the M.S. and Ph.D. degrees in physics from Virginia Tech, Blacksburg, in 1983 and 1985, respectively. He was a Research Associate with the University of Missouri—Columbia before moving to Utah State University (USU), Logan, in 1988. He is currently a Professor of physics at USU, where he leads the Materials Physics Group. He has worked in the area of electron scattering for his entire career and has focused on the electron emission and conductivity of materials related to spacecraft charging for the last two decades.

Todd Schneider received the B.S. degree in physics from Auburn University, Auburn, AL, in 1987. In 1988, he was with the Fusion Research Laboratory, Auburn University, where he contributed to the design and construction of the Compact Auburn Torsatron device. Since 1999, he has been with the NASA/Marshall Space Flight Center, Huntsville, AL. He is a member of the Environmental Effects Branch which tests spacecraft materials and systems in space environments created in the laboratory. He has performed work for numerous NASA programs including the International Space Station, James Webb Space Telescope, and Solar Probe Plus. In addition, he has conducted multiple Electrostatic Discharge Tests for corporations including Space Systems Loral and Emcore.

Charles W. Bowers received his Ph.D degree in physics from the Johns Hopkins University in 1985. He was a co-investigator with the Hopkins Ultraviolet Telescope mission (Astro-1) in 1990. He moved to the NASA Goddard Space Flight Center in 1993 as a member of the Space Telescope Imaging Spectrograph (STIS) team; STIS was installed and began operation on the Hubble Space Telescope in 1997. He is currently the Deputy Observatory Project Scientist for the James Webb Space Telescope.

Robert Meloy received the B.S.E. degree in electrical engineering from the University of South Florida in Tampa, FL, in 1981 and has spent most of his career developing space flight hardware for various NASA programs at Goddard Space Flight Center in Greenbelt, MD. He is currently a chief staff engineer with ASRC Federal Aerospace and Defense with focus on the James Webb Space Telescope project, specializing in spacecraft charging effects for that mission. He leads spacecraft charging effects efforts for other missions at Goddard as well.